JMEPEG (2011) 20:1078–1083
DOI: 10.1007/s11665-010-9731-0

1059-9495/$19.00

The Microstructural Evolution of Inconel Alloy 740 During Solution Treatment, Aging, and Exposure at 760 °C

Christopher J. Cowen, Paul E. Danielson, and Paul D. Jablonski

(Submitted July 9, 2010)

In this study, the microstructural evolution of Inconel alloy 740 during solution treatment and aging was characterized using optical and scanning electron microscopy. During double solution heat treatment, carbon is liberated from the dissolution of MC carbides during the first solution treatment at 1150 °C, and fine MC carbides are precipitated on gamma grain boundaries during the second solution treatment at 1120 °C. Due to the concurrent decrease in carbon solubility and the increase in the contribution of grain boundary diffusion at lower temperatures, the MC carbides on the gamma grain boundaries provide a localized carbon reservoir that aids in $M_{23}C_6$ carbide precipitation on gamma grain boundaries during exposure at 760 °C. The γ′ phase, which is the key strengthening phase in alloy 740, is incorporated into the alloy microstructure during aging at 850 °C. The main source of microstructural instability observed during exposure at 760 °C was the coarsening of the γ′ phase.

Keywords Inconel, microscopy, microstructure, superalloy

1. Introduction

Inconel alloy 740 is a nickel-based superalloy developed by Special Metals Corporation with the following nominal chemical composition: Ni-25Cr-20Co-0.5Mo-1.3Al-1.8Ti-1.5Nb-0.7Fe-0.3Mn-0.5Si-0.03C (wt.%) (Ref 1). This alloy is currently being evaluated for use as tubing and piping for steam boiler applications at Advanced-Ultra Supercritical (A-USC) steam conditions (Ref 2, 3). The target steam temperatures and pressures for USC plants are 760 °C and 35 MPa, respectively, which could possibly lead to power plant efficiencies up to 50%, depending upon boiler and steam turbine design and cooling approach (Ref 2, 3). These operating conditions preclude the use of materials found in supercritical and ultrasupercritical boiler construction, such as martensitic, ferritic, and austenitic stainless steels (Ref 4). Target in-service use times for tubing and piping in these coal-fired power plant environments are at least 100,000 h, with a minimum creep strength requirement of 100 MPa at 100,000 h at 760 °C and 35 MPa.

Alloy 740 is a γ′-strengthened, precipitation-hardenable superalloy. Its desirable constituent phases, in addition to the fcc gamma matrix, are the intermetallic $L1_2$-ordered γ′ phase, MC carbides, and complex $M_{23}C_6$ carbides. Undesirable phases such as the complex Si-rich G-phase, and the DO_{24}-ordered hexagonal Ni_3Ti-based η phase, have been observed in other heats of this alloy (Ref 5, 6). Being a γ′-strengthened alloy, the size, morphology, and volume fraction of γ′ phase in this alloy are extremely important microstructural features which directly influence, if not govern, the long-term microstructural, and thus, mechanical stability of alloy 740 under A-USC operating conditions. Due to the typical submicron size of the γ′ phase in nickel-based superalloys, microstructural characterization at the Scanning Electron Microscope (SEM) scale can be difficult, and Transmission Electron Microscopy (TEM) is the preferred imaging method used to characterize this phase.

In this study, the evolution of the microstructure of alloy 740 during solution heat treatment, aging, and isothermal exposure at 760 °C was characterized. A metallographic preparation route was developed with the intent of revealing γ′ for characterization at the SEM scale. The success of the metallographic preparation procedure led to the successful characterization of γ′ at the SEM scale. In addition, it was also possible to reveal the presence of γ′ in the microstructure optically under both darkfield and polarized light brightfield illumination conditions, prior to examination in the SEM.

2. Experimental

Prior to melt processing and fabrication, the phase constitution of alloy 740 was explored using the computational thermodynamics software package Thermo-Calc, with the Ni database (Ref 7) to gain insight into the predicted equilibrium constituent phases present within the alloy.

The particular alloy studied in this study was formulated, melted, cast, fabricated, and characterized in-house at the NETL-Albany foundry. After formulation from high purity raw materials, the alloy was Vacuum Induction Melted (VIM'ed) and cast into an approximately 7.8-kg cylindrical ingot.

Christopher J. Cowen, Paul E. Danielson, and **Paul D. Jablonski**, United States Department of Energy, National Energy Technology Laboratory, 1450 Queen Avenue SW, Albany, OR 97321. Contact e-mail: christopher.cowen@netl.doe.gov.

After removing the ingot hot top, a slice was removed to provide samples for chemical analysis. Subsequently, the surface of the ingot was conditioned, and the ingot was given a computationally optimized homogenization heat treatment (Ref 8). After homogenization, the ingot was then hot worked at approximately 1170 °C into plate form with a final thickness of 10.2 mm through a series of forging and rolling operations. The chemistry of the ingot was verified through x-ray Fluorescence at NETL-Albany and LECO analysis at Howmet Corporation.

In order to develop the appropriate microstructure for use in A-USC operating environments, samples were given the following solution heat treatment and aging treatment: 1150 °C/4 h/AC + 1120 °C/1 h/AC + 850 °C/16 h/AC. In order to chronicle the microstructural development that occurred during the two solution heat treatment steps, one sample was water quenched after undergoing the first solution treatment (1150 °C/4 h/WQ), and a separate sample was then water quenched after undergoing both solution treatments (i.e., 1150 °C/4 h/WQ + 1120 °C/1 h/WQ).

To observe the microstructural evolution that occurs in the absence of stress or steam environment at the A-USC target use temperature of 760 °C, solution-treated and aged samples were exposed at 760 °C in laboratory air for 500 and 1000 h.

Metallographic preparation of the samples consisted of grinding through 600 grit SiC abrasive, followed by a rough polish with a 9 μm diamond suspension, with a final polish with colloidal silica with an average particle size of 60 nm. The samples were then electrolytically etched using a potential ranging between 0 and 5 V DC in a solution of equal parts, by volume, of ethyl alcohol and concentrated HCl.

After metallographic preparation, the heat-treated microstructures were observed using a Leica DMR optical microscope and a FEI Inspect F Field Emission SEM. Brightfield (BF), darkfield (DF), and polarized light brightfield (PL) imaging modes were used for optical microscopy characterization. Secondary electron (SE) and backscattered electron (BSE) imaging modes were used for the SEM characterization. All of the images presented in this study were obtained from the longitudinal direction of the hot-rolled plate.

3. Results

Table 1 lists both the nominal and measured chemistry for the alloy 740 ingot produced at NETL-Albany.

Figure 1(a) and (b) show the Thermo-Calc-predicted weight fraction of all the equilibrium phases versus temperature for the nominal composition of alloy 740 as given in Table 1. The MC carbides in alloy 740 are predicted to exist over the temperature range of 775-1300 °C. The $M_{23}C_6$ carbides and the γ′ phase are observed to go into solution at 800 and 994 °C, respectively.

Figure 2(a)-(d) present optical and SEM images of the 1150 °C/4 h/WQ microstructure under different imaging conditions. Figure 2(a)-(c) show the same area at the same magnification under BF, DF, and PL illumination, respectively. A BSE image that illustrates the lack of grain boundary MC carbides is shown in Fig. 2(d).

Optical and SEM images of the 1150 °C/4 h/WQ + 1120 °C/1 h/WQ microstructure are shown in Fig. 3(a)-(d) under different imaging conditions. Figure 3(a)-(c) show the same area at the same magnification under BF, DF, and PL illumination, respectively. A BSE image that shows both intragranular and grain boundary MC carbides is shown in Fig. 3(d).

Figure 4(a)-(d) concludes the heat treatment schedule by presenting optical and SEM images of the 1150 °C/4 h/AC + 1120 °C/1 h/AC + 850 °C/16 h/AC microstructure under different imaging conditions. Figure 4(a)-(c) shows the same area at the same magnification under BF, DF, and PL illumination, respectively. Gamma grain and twin orientation is differentiated qualitatively by differences in color when imaged with PL illumination. The presence of γ′ due to etching interactions is visible in the DF and PL micrographs. A BSE image is shown in Fig. 4(d) which illustrates the difference in

Table 1 The nominal and actual chemistries of the Inconel 740 alloy produced at the NETL-Albany foundry

	Cr	Co	Mo	Nb	Ti	Al	Fe	Mn	Si	C
Nominal, wt.%	25	20	0.5	1.5	1.5	1.3	0.7	0.3	0.3	0.03
Actual, wt.%	24.67	19.98	0.50	1.47	1.47	1.23	0.62	0.30	0.29	0.03

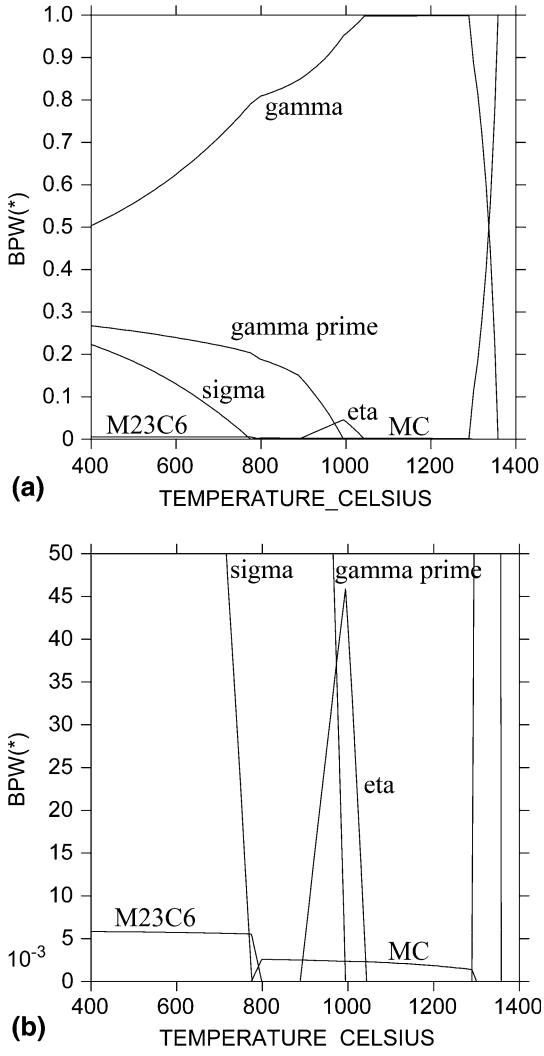

Fig. 1 Equilibrium weight fraction of phase vs. temperature for the nominal composition Ni-25Cr-20Co-0.5Mo-1.3Al-1.8Ti-1.5Nb-0.7Fe-0.3Mn-0.5Si-0.03C

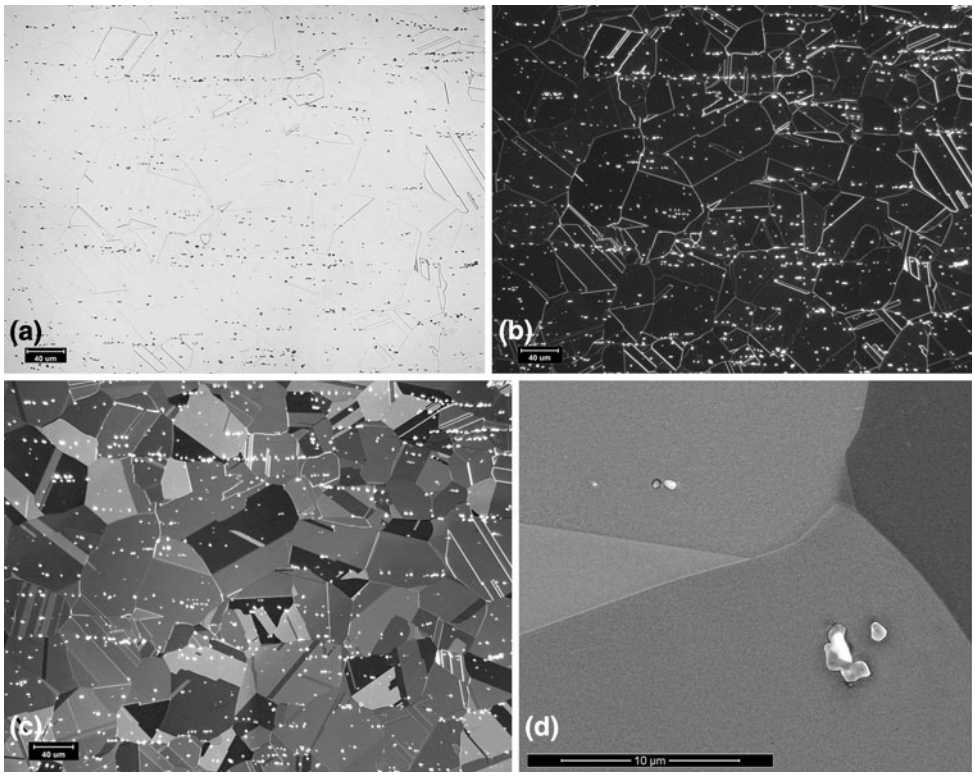

Fig. 2 The microstructure of alloy 740 after the 1150 °C/4 h/WQ heat treatment as viewed under different imaging conditions. The same area of the sample viewed under BF, DF, and PL illumination is presented in (a), (b), and (c), respectively. A BSE SEM image is shown in (d), in which MC carbides are present within the grains, but are not present on the gamma grain boundaries

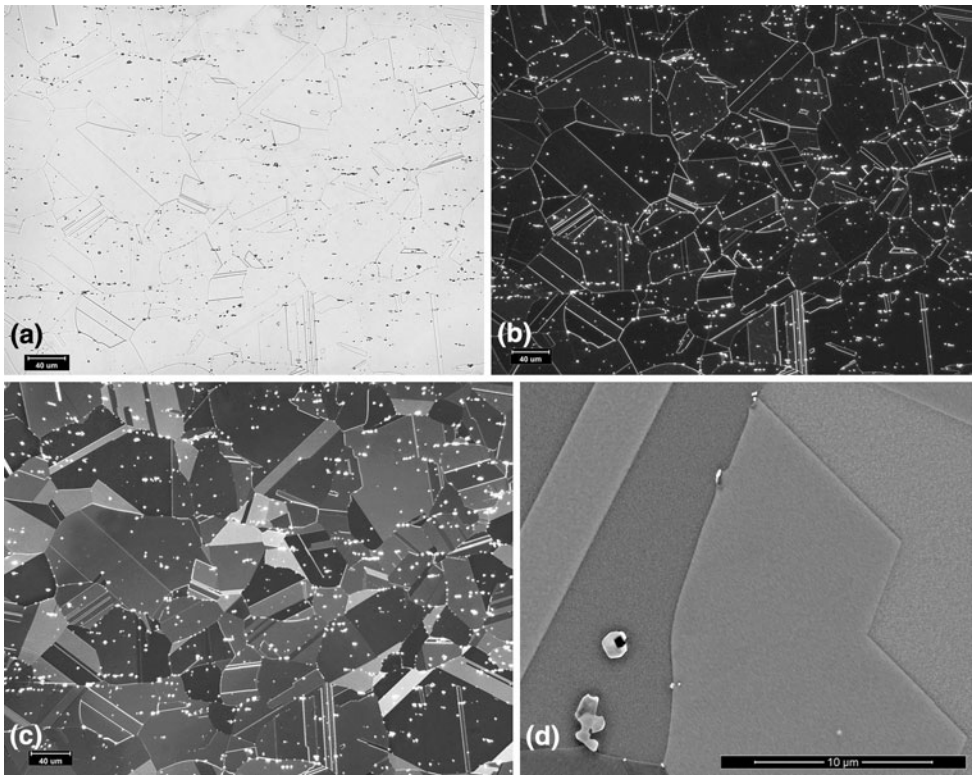

Fig. 3 The microstructure of alloy 740 after the 1120 °C/1 h/WQ heat treatment as viewed under different imaging conditions. The same area of the sample viewed under BF, DF, and PL illumination is presented in (a), (b), and (c), respectively. A BSE-SEM image is shown in (d). The MC carbides are visible within both the gamma grains and as fine precipitates on the gamma grain boundaries in (d), and exhibit similar contrast under BSE illumination

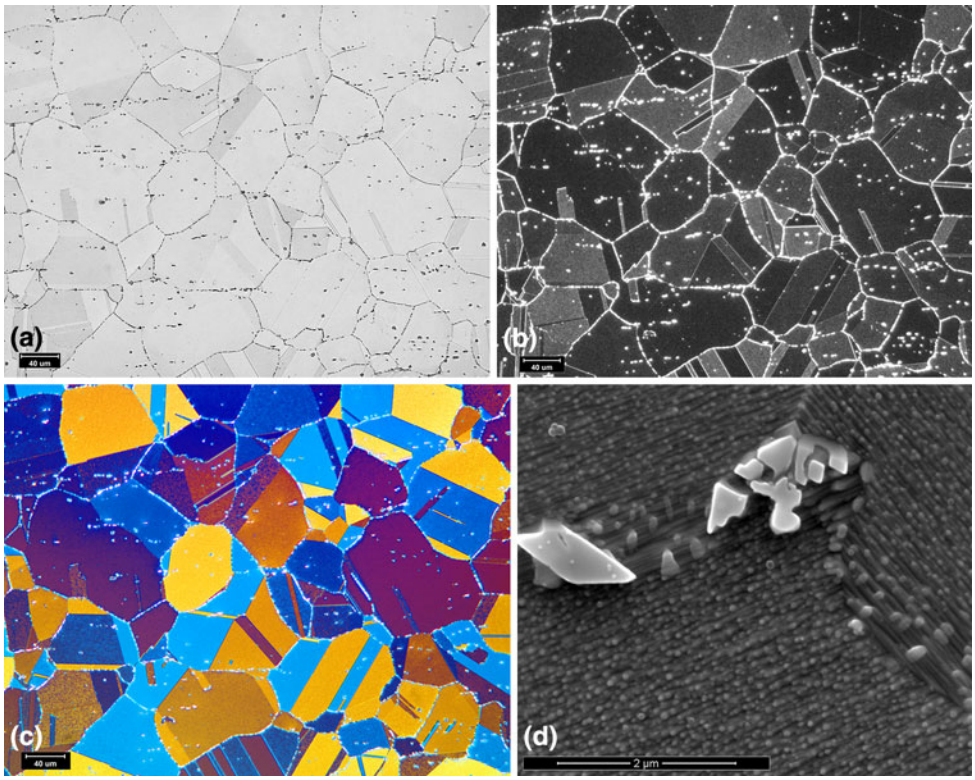

Fig. 4 The microstructure of alloy 740 after the 1150 °C/4 h/AC + 1120 °C/1 h/AC + 850 °C/16 h/AC heat treatment as viewed under different imaging conditions. The same area of the sample viewed under BF, DF, and PL illumination is presented in (a), (b), and (c), respectively. The color PL image in (c) shows gamma grain boundaries, gamma twin boundaries, gamma grain and twin orientation based on color and the presence of the γ′ phase. The BSE-SEM image in (d) illustrates γ′ morphology both near and away from the gamma grain boundaries

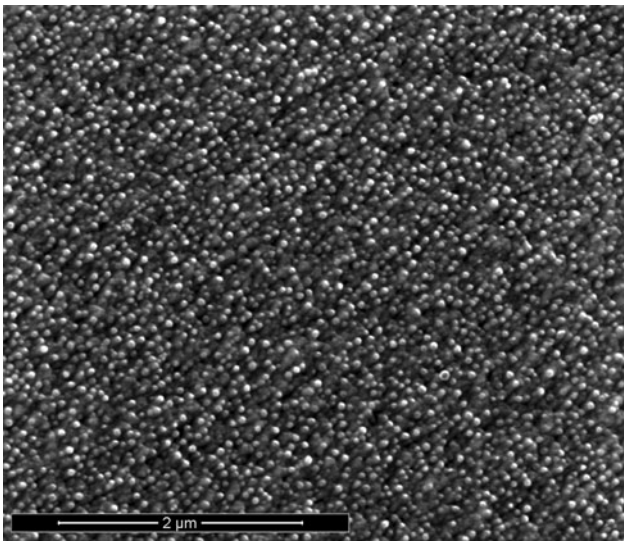

Fig. 5 An SE image that illustrates the size, volume fraction, and spherical morphology of γ′ observed within a gamma grain after the 1150 °C/4 h/AC + 1120 °C/1 h/AC + 850 °C/16 h/AC heat treatment

morphology observed for the γ′ phase both near and away from the gamma grain boundaries.

An SE image that illustrates the size, shape, and distribution of γ′ in alloy 740 after the double solutionizing and aging heat treatment is provided in Fig. 5.

Figure 6 provides the SE micrographs of the $M_{23}C_6$ carbides developed after 500- and 1000-h of exposure at 760 °C, while Fig. 7 shows SE micrographs that illustrate γ′ coarsening and morphology transitions after the same exposure duration.

4. Discussion

4.1 Microstructural Evolution During Solution Treatment

After the first solution heat treatment at 1150 °C, the microstructure of alloy 740 consists of equiaxed gamma grains and a dispersion of MC carbides within these grains. In the absence of crystallographic diffraction data, these carbides are most probably MC-based. This supposition is based in part upon the Thermo-Calc equilibrium phase predictions shown in Fig. 1. In addition, their bright contrast when imaged in BSE mode suggests the presence of electronically dense elements with a similar morphology and measured composition to MC carbides characterized in alloy 740 by Evans et al. (Ref 6).

From energy dispersive x-ray analysis (EDX) measurements in the SEM, the main metallic constituents of the MC carbides were found to be Ti and Nb. The Ti and Nb concentrations within the MC carbides were approximately equal in atomic percent, which suggests a phase chemistry of $(Ti_{0.5}Nb_{0.5})C$. The MC carbides in this microstructure occur intragranularly, and are only randomly found on gamma grain boundaries or twin boundaries. The random distribution of MC carbides occurs in this manner due to the fact that they crystallize from the melt

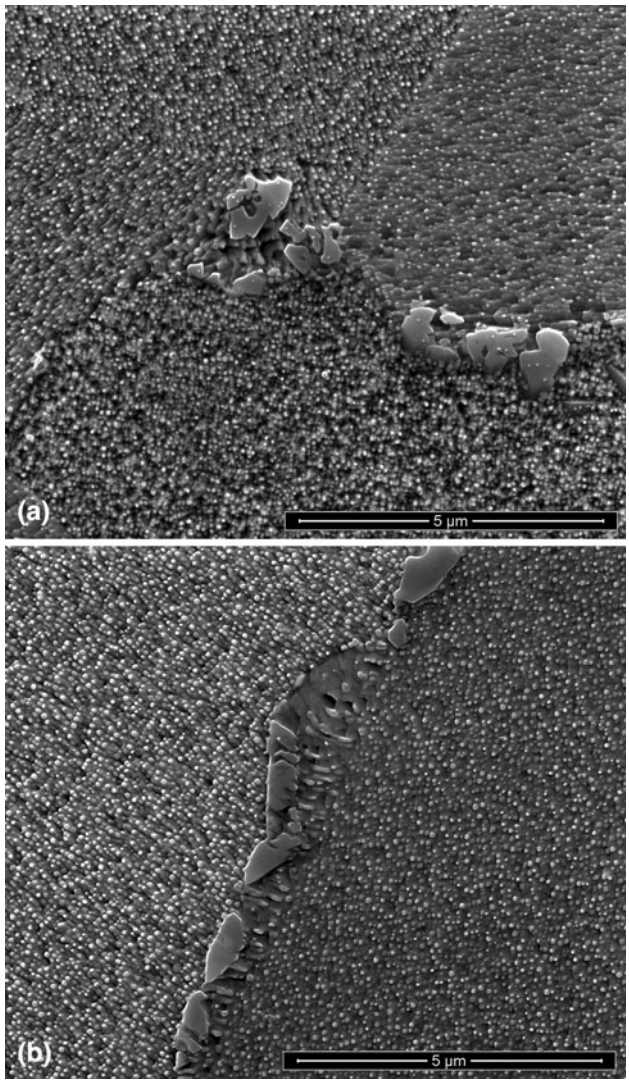

Fig. 6 Secondary electron images of the solution treated and aged microstructure after exposure at 760 °C for (a) 500 h, and (b) 1000 h

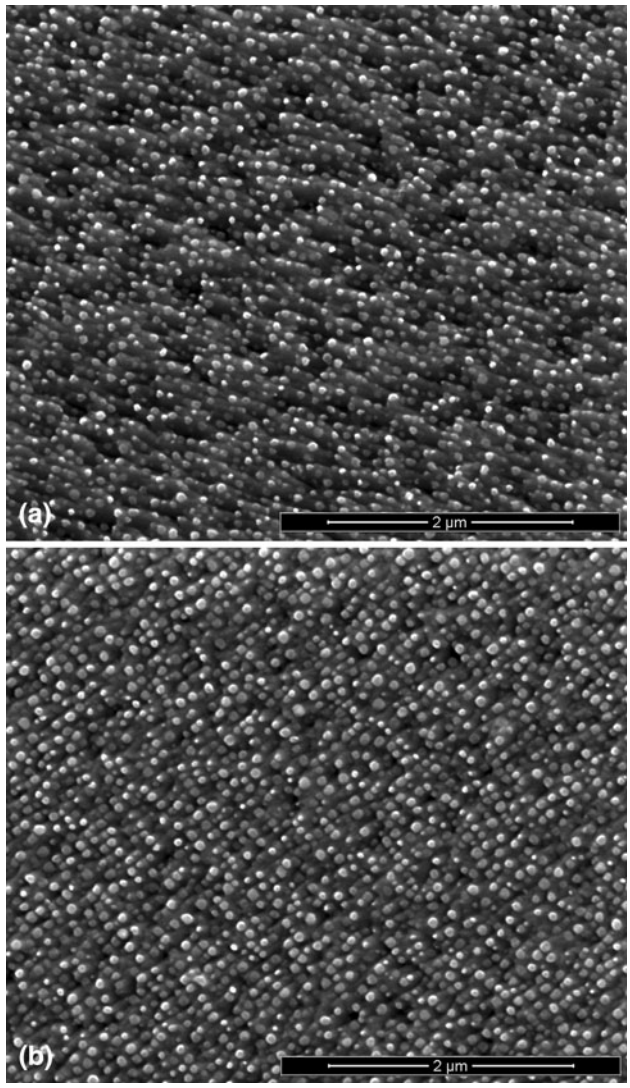

Fig. 7 The size, shape, and distribution of γ′ within a gamma grain after (a) 500, and (b) 1000 h at 760 °C

during the initial stages of solidification, and remain within the microstructure throughout all stages of thermal-mechanical processing. The alignment of the MC carbides parallel with the rolling direction is then an expected occurrence, and is readily visible in the optical micrographs in Fig. 2-4. Annealing twins within the gamma grains are very prevalent in alloy 740, but are not preferential sites for the location of MC carbides after solutionizing at 1150 °C.

The second solution heat treatment at 1120 °C plays an important role in preparing the microstructure for aging at 850 °C and subsequent 760 °C service. During this heat treatment step, very fine MC carbides nucleate (i.e., fine in comparison to those carbides already present from melt processing) directly on the gamma grain boundaries. Compare the BSE images in Fig. 2(d)-3(d). These finely precipitated grain boundary carbides also appear to be MC carbides based on the Thermo-Calc phase predictions shown in Fig. 1, and the fact that they posses similar chemical contrast to the MC carbides present since melt processing when BSE imaged. Consequently, it seems that the first 4-h-solutionizing heat treatment at 1150 °C serves to distribute carbon into the gamma matrix from the partial dissolution of the MC carbides. The second solution treatment, i.e., 1 h at 1120 °C, then utilizes the carbon liberated during the first solution treatment to nucleate and grow MC carbides at the gamma grain boundaries. Since an excess of carbon would be expected at the grain boundaries, the solubility of carbon is reduced with decreased temperature. Thus, the contribution of grain boundary diffusion to the total diffusion always increases with decreasing temperature, leading to the conclusion that the role of the second solutionizing step is to nucleate the MC carbides on the gamma grain boundaries. Nucleating MC carbides on the gamma grain boundaries, therefore, localizes the carbon source on the gamma grain boundaries. In addition, any residual carbon left within the gamma matrix for the $M_{23}C_6$ carbides which precipitate during exposure at 760 °C can also contribute. Since the $M_{23}C_6$ carbides in alloy 740 have been observed in this study and the study of others (Ref 5, 6) to only reside on the gamma grain boundaries or twin boundaries, they play a crucial role in locking the movement of gamma grain boundaries due to migration and grain boundary sliding during creep deformation during service. Therefore, the second solution heat treatment

performed prior to the aging heat treatment is an important step in producing a microstructure that will exhibit the best performance under USC operating conditions.

4.2 Microstructural Evolution During Aging

Aging at 850 °C serves the purpose of precipitating γ′ within the gamma matrix while avoiding the precipitation of both the undesirable σ and η phases (see Fig. 1). Figure 5 illustrates the size, shape, and distribution of the γ′ within gamma grains as well as near the gamma grain boundaries. The γ′ observed away from the gamma grain boundaries at the SEM scale in the solution treated and aged condition possessed a spherical morphology, which implies strong coherency between γ′ and the matrix and a low degree of mismatch between the lattice parameters of both phases (Ref 9). The observable γ′ area fraction in alloy 740 was dependent upon the different electrolytic etching rates of the gamma grains which formed the continuous matrix around the discontinuous γ′ precipitates; this coupled grain orientation/etching effect is illustrated when comparing the areal distribution of the γ′ within the three gamma grains in Fig. 5, and by the subtle differences in color shown within gamma grains and twins in the PL image in Fig. 3(c).

4.3 Microstructural Evolution During Exposure at 760 °C

Figure 6(a) and (b) show SE images of the solution-treated and aged microstructure of alloy 740 after exposure to laboratory air at 760 °C for 500 and 1000 h, respectively. (The $M_{23}C_6$ carbides are visible on the gamma grain boundaries in both micrographs.) The precipitation of the $M_{23}C_6$ carbides in alloy 740 occurs during exposure at 760 °C, which agrees with both their absence from the microstructure of samples aged at 850 °C and the Thermo-Calc results that predict these carbides to go into solution at 800 °C. From EDX analysis, the main metallic constituents of the $M_{23}C_6$ carbides, in order from highest concentration to lowest concentration, were found to be Cr, Ni, and Co, respectively. In comparison to the EDX spectra obtained from the MC carbides, the spectra obtained from the $M_{23}C_6$ carbides exhibited Ti and Nb contents less than or equal to 1.5 atomic percent. The dark contrast of the $M_{23}C_6$ carbides in comparison to the bright contrast of the MC carbides when imaged in BSE mode agrees well with the lack of Ti, and especially Nb, as measured in the $M_{23}C_6$ carbides. The $M_{23}C_6$ carbides were found to exist only on gamma grain boundaries, or twin boundaries, after exposure at 760 °C. This is expected due to the reduced solubility of Cr and carbon with reduced temperature. The presence of fine MC carbides that developed on the grain boundaries during the 1120 °C solution treatment act as an additional local carbon source, along with the strong contribution of grain boundary diffusion at temperatures in range of 50-60% of the melting temperature.

The coarsening of γ′ with increased exposure from 500 to 1000 h at 760 °C was the source of microstructural instability observed. Figure 7 shows the size, shape, and distribution of γ′ within a gamma grain after 500 and 1000 h at 760 °C. Comparing Fig. 5 and 7, it is clear that γ′ has coarsened with increased exposure time in the absence of applied stress. The transition from a spherical shape to more of a cubic morphology is displayed in conjunction with the observed coarsening, and more γ′ precipitates were observed to display this morphology transition with increased exposure time from 500 to 1000 h. The instability observed in the form of coarsening with increased exposure time, and the morphology transition observed at the SEM scale, have adverse implications for achieving microstructural stability for times greater than or equal to 100,000 h at 760 °C. The addition of an applied creep stress during use in service would be expected to accelerate any observed instability in the microstructure, and introduce potential rafting of the γ′ precipitates.

5. Conclusions

1. During a double solution heat treatment, carbon is liberated from the partial dissolution of MC carbides during the first solution treatment at 1150 °C and fine MC carbides are precipitated on gamma grain boundaries during the second solution treatment at 1120 °C.
2. Aging at 850 °C precipitates γ′ within the gamma matrix while avoiding the precipitation of both the undesirable σ and η phases.
3. The precipitation of the $M_{23}C_6$ carbides in alloy 740 occurs during exposure at 760 °C. The γ′ precipitates in alloy 740 coarsen with increased exposure time at 760 °C in the absence of an applied stress. The transition onset from a spherical to a cubic morphology is displayed in conjunction with the observed coarsening, and more precipitates were observed to display this morphological transition with increased exposure time from 500 to 1000 h.

Acknowledgments

The authors would like to thank Ed Argetsinger and Marisa Arnold of NETL-Albany for their assistance with thermomechanical processing and XRF chemical analysis.

References

1. Available online at: http://www.specialmetals.com/documents/Inconel%20alloy%20740.pdf
2. R. Viswanathan, A.F. Armor, and G. Booras, A Critical Look at Supercritical Power Plants, *Power Magazine*, 2004, April Issue, p 42–49
3. G.R. Holcomb, Superalloys For Ultrasupercritical Steam Turbines—Oxidation Behavior, *Superalloys 2008*, R.C. Reed, K.A. Green, P. Caron, T. Gabb, M.G. Fahrmann, E.S. Huron, and S.A. Woodard, Ed., The Minerals, Metals, and Materials Society, Warrendale, PA, 2008, p 601–607
4. R. Viswanathan and W. Bakker, Materials for Ultrasupercritical Coal Power Plants—Boiler Materials: Part 1, *J. Mater. Eng. Perform.*, 2001, **10**, p 81–95
5. S. Zhao, X. Xie, G.D. Smith, and S.J. Patel, Microstructural Stability and Mechanical Properties of a New Nickel-Based Superalloy, *Mater. Sci. Eng. A*, 2003, **355**, p 96–105
6. N.D. Evans, P.J. Maziasz, R.W. Swindeman, and G.D. Smith, Microstructure and Phase Stability in INCONEL Alloy 740 During Creep, *Scripta Mater.*, 2004, **51**, p 503–507
7. *Ni-DATA, version 7*, Sente Software Ltd., Surrey Technology Centre, UK, 2005
8. P.D. Jablonski and C.J. Cowen, Homogenizing a Nickel-Based Superalloy: Thermodynamic and Kinetic Simulation and Experimental Results, *Metall. Mater. Trans. B*, 2009, **40**, p 182–186
9. C.T. Sims, N.S. Stoloff, and W.C. Hagel, *Superalloys II*, John Wiley and Sons, New York, NY, 1987